

Quadrangulating a Mesh using Laplacian Eigenvectors

Shen Dong¹ Peer-Timo Bremer¹ Michael Garland¹ Valerio Pascucci² John C. Hart¹

¹University of Illinois at Urbana-Champaign ²Lawrence Livermore National Laboratory
 {shendong, ptbremer, garland, hart}@uiuc.edu pascucci@llnl.gov

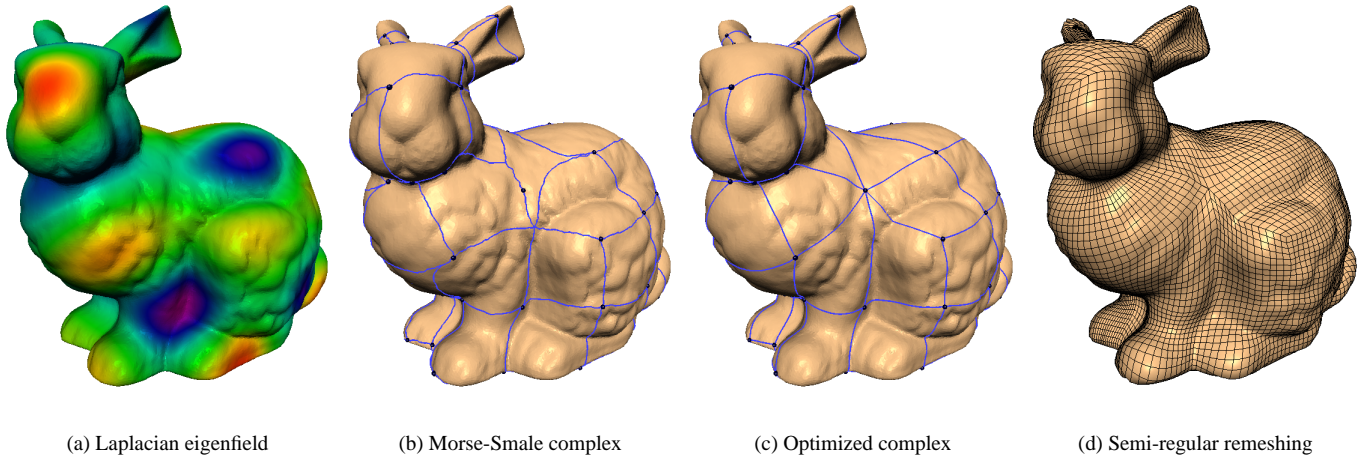


Figure 1: We quadrangulate a given triangle mesh by extracting the Morse-Smale complex of a selected eigenvector of the mesh Laplacian matrix. After optimizing the geometry of the base complex, we can generate a semi-regular remeshing of the bunny.

Abstract

Resampling raw surface meshes is one of the most fundamental operations used by nearly all digital geometry processing systems. The vast majority of work in the past has focused on triangular remeshing; the equally important problem of resampling surfaces with quadrilaterals has remained largely unaddressed. Despite the relative lack of attention, the need for quality quadrangular resampling methods is of central importance in a number of important areas of graphics. Quadrilaterals are the preferred primitive in many cases, such as Catmull-Clark subdivision surfaces, fluid dynamics, and texture atlasing.

We propose a fundamentally new approach to the problem of quadrangulating manifold polygon meshes. By applying a Morse-theoretic analysis to the eigenvectors of the mesh Laplacian, we have developed an algorithm that can correctly quadrangulate any manifold, no matter its genus. Because of the properties of the Laplacian operator, the resulting quadrangular patches are well-shaped and arise directly from intrinsic properties of the surface, rather than from arbitrary heuristics. We demonstrate that this quadrangulation of the surface provides a base complex that is well-suited to semi-regular remeshing of the initial surface into a fully conforming mesh composed exclusively of quadrilaterals.

Keywords: quadrangular remeshing, spectral mesh decomposition, Laplacian eigenvectors, Morse theory, Morse-Smale complex

1 Introduction

Polygon meshes, especially those arising from scanning systems and isosurface extraction, frequently exhibit a number of deficien-

cies. They are often sampled at inappropriate resolutions and typically contain many poorly shaped elements. Because of the constant occurrence of poor meshes, the ability to partition surfaces into well-shaped regions and to resample surfaces with well-formed meshes is of critical importance in almost all mesh processing systems.

The vast majority of prior work on remeshing methods in the graphics literature has focused on the problem of producing triangle meshes. However, the ability to produce high-quality quadrilateral meshes is often just as important. Quadrilaterals are the preferred choice of primitive for many man-made objects, such as buildings, and for most character models. Quadrilaterals are also the preferred primitive in several simulation domains, including computational fluid dynamics. Many subdivision surface formulations, notably Catmull-Clark surfaces, and spline patch primitives, such as NURBS, require quadrangular base complexes. Furthermore, decomposing a surface into well-shaped quadrangles provides a natural means of building texture atlases. Nevertheless, only recently have methods been developed for automatically quadrangulating complex surfaces. Those few methods which do exist are frequently quite complex, delicate to implement, and rely on a carefully tuned balance of multiple heuristic components. And several recently proposed methods produce only quad-dominant—rather than pure quadrilateral—meshes, making them ill-suited for use in creating Catmull-Clark base domains.

In this paper, we present a fundamentally new approach for building quadrangular base complexes over triangulated manifolds of arbitrary genus. In contrast to heuristic clustering-based approaches, our quadrangulation arises out of the intrinsic properties of the initial surface shape. We use this quadrangulation of the surface as the basis for a semi-regular remeshing system that produces fully conforming meshes composed exclusively of quadrilaterals and with a generally small number of extraordinary points. We also demon-

strate that our quadrangular complexes produce high quality results when used to define Catmull-Clark subdivision surfaces.

To decompose a surface into quadrangular patches, we introduce a new Morse-theoretic analysis of the spectrum of the target mesh. We use the eigenvectors of a discrete Laplacian matrix to define scalar fields over a surface mesh such that the extrema of a given field occur at a desired “frequency.” Extracting the Morse-Smale complex of these scalar fields provides us with a decomposition of the surface that is guaranteed to be quadrangular on even the most topologically complex surfaces.

2 Related Work

A given mesh represents an inherently fixed sampling of some underlying shape, decomposing it into a fixed collection of polygons. Clearly, this fixed sampling will not in general provide a *desirable* sampling for all applications. Consequently, repartitioning and/or resampling an existing mesh is one of the most fundamental tools necessary in any mesh processing system. This touches on a number of closely interrelated problems, all of which have been extensively studied. We review only the most relevant results here.

2.1 Parameterization & Partitioning

Given a surface patch homeomorphic to a disk, there are many methods available for automatically constructing a mapping of that patch into the plane [Floater and Hormann 2004]. Once such a mapping is established, the patch may be trivially resampled on a regular parametric grid. This is the fundamental approach underlying the construction of geometry images [Gu et al. 2002; Sander et al. 2003]. Assuming that the parametric distortion is sufficiently low, this approach can produce a reasonable resampling of the surface.

Manifolds of other topological type must in general be partitioned into patches homeomorphic to a disk prior to being parameterized. Decomposing the mesh into patches can also be used to dramatically reduce the overall level of parametric distortion. Common approaches to the problem of surface partitioning include iterative merging [Garland et al. 2001], minimum graph cuts [Katz and Tal 2003], and generalized Lloyd relaxation [Sander et al. 2003].

2.2 Remeshing

Surface meshes produced by automatic reconstruction systems are often ill-suited for subsequent processing steps. Their sampling density is frequently insensitive to the underlying shape, and they often tend to exhibit undesirable artifacts such as high valence vertices, very small or very large angles, poor edge length distributions, etc. Consequently, many remeshing methods have been developed to correct these various deficiencies.

Mesh Simplification. Meshes constructed from point cloud data, range scans, and isosurface extraction are almost invariably over-tessellated. The target shape can almost always be represented very well using far fewer polygons. Many surface simplification methods have been developed to derive such simpler approximations automatically [Garland 1999]. The majority of simplification algorithms operate by greedily applying a decimation primitive, such as edge contraction [Hoppe 1996; Garland and Heckbert 1997] or vertex removal [Schroeder et al. 1992]. A more general approach

is to iteratively apply operations such as edge contraction and flipping within a global optimization search [Hoppe et al. 1993]. These methods focus primarily on adapting the mesh connectivity; retiling methods, in contrast, explicitly resample vertex sites and subsequently tessellate the chosen vertices [Turk 1992]. A similar emphasis on directly resampling the surface can be seen in methods that construct a global decomposition of the surface into patches, which are then polygonized to produce a final mesh [Kalvin and Taylor 1996; Cohen-Steiner et al. 2004].

Semi-regular Remeshing. The overriding concern of simplification methods is to reduce mesh complexity while maintaining geometric fidelity; quality measures such as vertex degree and mesh regularity are generally ignored. For a host of multiresolution mesh analysis methods the paramount concern is instead that the mesh have the greatest possible regularity (e.g., triangle meshes with degree 6 vertices). Such regular mesh structure is important, in part, because it can be derived by recursive mesh subdivision operations.

Semi-regular remeshing schemes approach this problem as a two step process. First, they decompose the surface into a set of triangular or quadrangular patches. Second, they resample each patch by recursive subdivision. Eck *et al.* [1995] used the dual of a quasi-Voronoi decomposition to create a set of triangular base patches. In a similar vein, the MAPS system [Lee et al. 1998] builds a triangular base domain via simplification. Both are designed for use as the initial stage in a pipeline for wavelet or subdivision analysis of surfaces. More recently, this fundamental approach has been extended by the normal meshes construction [Guskov et al. 2000; Friedel et al. 2004], which focuses primarily on the encoding efficiency of the multiresolution hierarchy, and globally smooth parameterization [Khodakovskiy et al. 2003], which produces a higher degree of parametric smoothness across triangular patch boundaries.

In contrast to the triangular case, comparatively little work has been done on the problem of constructing semi-regular quadrilateral meshes. The most common approach that others have taken is to construct a non-quadrangular decomposition, from which a quadrangulation can be derived. Eck and Hoppe [1996] begin by constructing a triangular base complex. They then solve a maximum matching problem over the dual graph of this complex, joining all paired triangles into quadrangles. Similarly, Boier-Martin *et al.* [2004] produce an arbitrary clustering of the surface into connected face sets, whose boundaries may be polygons of any type, and then quadrangulate these polygons.

Isotropic Remeshing. Applications that are unconcerned with multiresolution analysis may desire well-sampled meshes without the need for the regularity constraints imposed by semi-regular remeshing schemes. Isotropic remeshing methods meet this need by producing triangular meshes which consist of (roughly) equilateral elements and whose vertices obey a specified density function.

Alliez *et al.* [2002] proposed one natural solution to this problem: compute a conformal parameterization of the surface, distribute vertices in the parameter domain suitably, and compute their Delaunay triangulation. In a follow-on to this work [Alliez et al. 2003b] they demonstrate that weighted centroidal Voronoi diagrams, which they construct via Lloyd relaxation, provide a powerful means of generating a good vertex distribution. Surazhsky and Gotsman [2003] developed an alternative approach that uses only local mesh updates and therefore requires no global parameterization. Their approach can also be used to adapt the weighted centroidal Voronoi diagrams of Alliez *et al.* [Alliez et al. 2003b] to work efficiently on much larger meshes [Surazhsky et al. 2003].

Anisotropic Remeshing. In certain cases, meshes whose element aspect ratios conform to an appropriate tensor field can be more desirable than purely isotropic meshes. For example, meshes which sample a shape optimally will have elements which stretch out in directions of low curvature and are compressed in directions of high curvature. Similarly, certain fluid flow simulations are most robust when elements conform to the expected flow directions.

This anisotropy arises most naturally in the context of generating quadrangular meshes since quadrilaterals, as opposed to triangles, tend to have an obviously preferred orientation. Several methods have been proposed very recently for generating anisotropic quad-dominant (i.e., primarily, but not exclusively, composed of quadrilaterals) meshes. Alliez *et al.* [2003a] numerically compute integral lines of the two principal direction fields of the surface in a conformal parametric domain. The spacing of these lines is controlled by the local surface curvature, and vertices are created where two orthogonal lines intersect. The stability of this method hinges on carefully smoothing the curvature tensor field from which the principal directions are derived. Marinov and Kobbelt [2004] demonstrate how this approach can be made to work without the need for a parameterization of the surface. Dong *et al.* [2005] similarly adopt the idea of tracing orthogonal families of curves, but they define these curves using a harmonic scalar field defined over the surface.

Mesh Generation. There is an extensive literature on the generation of meshes for use in numerical simulation frameworks such as the finite element method [Bern and Eppstein 1995; Owen 1998]. Such methods tend to emphasize bounds on minimum/maximum angles and edge lengths, as these quantities are usually tied to the convergence rate of their numerical methods. Within the mesh generation community, a number of techniques have been developed for generating quadrilateral or quad-dominant meshes over planar domains. The most common techniques in widespread use are advancing front methods, such as paving [White and Kinney 1997], and methods which transform triangulations into quad meshes [Shimada *et al.* 1998; Owen *et al.* 1999].

2.3 Surface Analysis

Spectral Graph Theory. The eigenvalues/eigenvectors of the discrete Laplacian matrix provide a natural formulation of the *spectrum* of a graph, and hence a mesh. They generalize the discrete cosine transform in the plane and spherical harmonics on the sphere. The study of this eigenspace—known as spectral graph theory—is a well-developed branch of mathematics and has produced many fascinating results [Chung 1997].

As the spectral decomposition of a mesh exposes a great deal of its structure, it has been successfully applied in many diverse ways. It defines a natural frequency domain over the mesh, and hence provides an attractive formalism for surface smoothing and mesh signal processing [Taubin 2000]. Retaining and quantizing only the most important frequency bands provides a very effective means for compressing the surface geometry [Karni and Gotsman 2000]. The eigenvector corresponding to the first non-zero eigenvalue—the Fiedler vector—has been used with great success for graph bisection [Hendrickson and Leland 1995]. Similarly, it can be used to provide a high-locality ordering for mesh data [Isenburg and Lindstrom 2004] or, more generally, to solve the “seriation” problem [Atkins *et al.* 1999]. The Fiedler vector, together with the subsequent eigenvector, can be used to automatically embed graphs into the plane in an aesthetically pleasing manner [Koren *et al.* 2002].

Morse Theory. Elements of Morse theory date back to the 19th century [Cayley 1859; Maxwell 1870] but developed more thoroughly later, first for continuous functions on smooth manifolds [Morse 1925; Milnor 1963], and more recently (and more usefully) for meshes [Banchoff 1967; Edelsbrunner *et al.* 2003]. In computer graphics, Morse theory and its related topological data structures have been applied to implicit surfaces [Stander and Hart 1997], volumetric isosurfaces [van Kreveld *et al.* 1997; Pascucci and Cole-McLaughlin 2002; Weber *et al.* 2002], surface meshes [Ni *et al.* 2004] and shape database searches [Hilaga *et al.* 2001].

We use the Morse-Smale complex as an initial quadrangulation of a meshed surface, using as a Morse function one of the Laplacian eigenvectors. Our construction of the Morse-Smale complex is the same as has been used previously [Bremer *et al.* 2004]. Our contribution is instead the application of Morse analysis to a shape harmonic which appears to be unique at least within the graphics community.

3 Theoretical Background

We assume that we are given an initial triangulated manifold mesh $M = (V, F)$ with vertex set V and triangle set F . The manifold M may be of any genus, but to simplify our presentation, we shall assume that M has a single connected component.

Our approach to quadrangulating this input manifold is grounded in a Morse-theoretic analysis of the Laplacian spectrum of piecewise linear manifolds. In this section, we review the theoretical underpinnings of our method. We will present the details of our quadrangulation algorithm in Section 4.

3.1 Morse Theory on 2-Manifolds

Let us suppose for the moment that M is a continuous 2-manifold embedded in \mathbb{R}^3 . Since M is a manifold, there exists a local u, v parameterization in a neighborhood of each point $p \in M$. Let $f : M \rightarrow \mathbb{R}$ be a twice differentiable scalar function. A point $c \in M$ is called *critical* if $f_u(c) = f_v(c) = 0$, with *critical value* $f(c)$. The critical point c is *degenerate* if $f_{uu}(c)f_{vv}(c) - 2f_{uv}(c) = 0$, otherwise it is *Morse*. The function f is *Morse* if all its critical points are Morse.¹

Let $\lambda_1 \leq \lambda_2$ be the two eigenvalues² of the Hessian of f , with corresponding eigenvectors $(\mathbf{e}_1, \mathbf{e}_2)$. The number of negative eigenvalues classifies a Morse critical point as a *minimum* (zero), *saddle* (one) or *maximum* (two).

Every *regular* (non-critical) point $p \in M$ has a well defined gradient $\nabla f(p) = (f_u(p), f_v(p))$. From p we can integrate this gradient in both directions tracing out an *integral line* $\gamma : \mathbb{R} \rightarrow M$ as the maximal solution of the ODE $\gamma'_s(s) = \nabla f(\gamma(s))$ with initial value $\gamma(0) = p$. The *origin* $\text{org } \gamma = \lim_{s \rightarrow -\infty} \gamma(s)$ and *destination* $\text{dest } \gamma = \lim_{s \rightarrow \infty} \gamma(s)$ of an (open) integral line γ are distinct critical points and neither is included in γ . Two integral lines are either disjoint or identical and the set of integral lines covers M except for the critical points. The manifold M is thus the disjoint union of the integral lines and the critical points of f .

¹Strictly speaking, the Morse distinction has classically required the function to have unique critical values which simplifies the topological surgery when processing their corresponding topological events in value order, but is otherwise not necessary. Morse critical points are nevertheless necessarily isolated [Milnor 1963].

² $(\lambda_1, \lambda_2) = \frac{1}{2}(f_{uu} + f_{vv} \pm \sqrt{4f_{uv}^2 + (f_{uu} - f_{vv})^2})$.

A 2-manifold Morse function f is *Morse-Smale* if no integral line both starts and ends at a saddle. Almost all Morse functions are Morse-Smale but the classical example of altitude on a vertically oriented torus is *not*, since some of its integral lines originate and terminate at saddles. Each integral line of a Morse-Smale function is either an *ascending separatrix* if its origin is a saddle and destination is a maximum, a *descending separatrix* if its destination is a saddle and origin is a minimum, or *simple* if its origin is a minimum and destination is a maximum.

A Morse-Smale function f provides a cellular decomposition of M into a *Morse-Smale complex* whose 0-cells are the critical points of f , 1-cells connecting critical points are the four separatrices starting and ending each saddle, and 2-cells are the remaining disjoint regions of M . Each region is a quadrilateral whose boundary is a saddle ascending to a maximum, descending to a saddle, descending to a minimum and ascending to the original saddle. It is generically possible that the two saddles are identical, causing the two ascending or descending sides of the quadrilateral to merge.

The Morse-Smale complex can also be defined for 2-manifold triangle meshes, by extending Morse theory to the piecewise linear function resulting from the linear interpolation of pre-assigned unique vertex values across the edges and faces of the mesh. An arbitrary but consistent ordering (such as the vertex index or a hash of position) can be used to perturb non-unique vertex values [Edelsbrunner and Mücke 1990]. Critical points are then classified based on their local neighborhood [Banchoff 1967; Edelsbrunner et al. 2003]. If all edge-connected neighbors of a point c have a lower function value, c is called a maximum; if all are above, a minimum; and if the function changes between above and below four times c is classified as a (simple) saddle, see Figure 2. In general, there can exist saddles with an arbitrary number of switches, which are split into a collection of simple saddles.

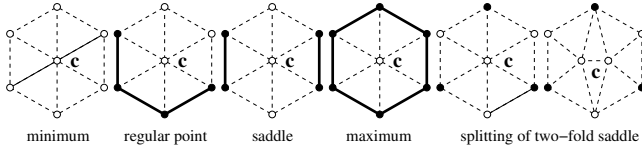


Figure 2: Classification of a vertex c based on relative height of its neighbors. Light vertices/edges mark higher-value neighbors and solid vertices/edges lower-value neighbors.

For the analysis of piece-wise linear functions integral lines are replaced by lines of steepest ascent or descent. Note that, unlike integral lines steepest lines are not uniquely defined and not necessarily disjoint. However, Edelsbrunner *et al.* [2003] showed that there always exists a set of steepest lines which can be simulated as pair-wise disjoint and which, using the definitions of the smooth case, define a non-degenerate Morse-Smale complex. Section 4.2 describes the implementation of this algorithm further, summarizing Bremer *et al.* [2004].

3.2 Spectral Analysis of Meshes

It is well-known that the discrete Laplacian operator on piecewise linear functions over triangulated manifolds is given by:

$$\Delta f_i = \sum_{j \in N_i} w_{ij}(f_j - f_i), \quad (1)$$

where N_i is the set of vertices adjacent to vertex i and w_{ij} is a scalar weight assigned to the directed edge (i, j) . For graphs free of

any geometry embedding, it is customary to use the combinatorial weights $w_{ij} = 1/\deg(i)$ in defining this operator. However, for 2-manifold surfaces the appropriate choice are the discrete harmonic weights:

$$w_{ij} = -\frac{1}{2}(\cot \alpha_{ij} + \cot \beta_{ij}). \quad (2)$$

Here α_{ij} and β_{ij} are the angles opposite the edge (i, j) . Details on the derivation of these weights can be found in several sources [Pinkall and Polthier 1993; Duchamp et al. 1997; Desbrun et al. 1999].

This formulation of the Laplacian is clearly a linear operator. If we represent the function f by the column vector of its values at all vertices $\mathbf{f} = [f_1 \ f_2 \ \dots \ f_n]^T$, we can reformulate the Laplacian as a matrix

$$\Delta \mathbf{f} = -\mathbf{L}\mathbf{f}, \quad (3)$$

where the Laplacian matrix \mathbf{L} has entries

$$L_{ij} = \begin{cases} \sum_k w_{ik} & \text{if } i = j, \\ -w_{ij} & \text{if } (i, j) \text{ is an edge of } M, \\ 0 & \text{otherwise.} \end{cases} \quad (4)$$

The eigenvalues $\lambda_1 = 0 \leq \lambda_2 \leq \dots \leq \lambda_n$ of \mathbf{L} form the *spectrum* of the mesh M and the corresponding eigenvectors $\mathbf{e}_1, \mathbf{e}_2, \dots, \mathbf{e}_n$ of \mathbf{L} define piecewise linear functions over M of progressively higher frequencies [Taubin 2000].

4 Building a Quadrangular Base Complex

Recall that our goal is to construct a *quadrangulation* of the input mesh M . We want this quadrangulation to be pure, in the sense that it contains no non-quadrangular patches, and we want it to be well-defined no matter the genus of the input. We would also like each quadrangular patch to be well-shaped.

As outlined in Section 3.1, the Morse-Smale complex of a piecewise linear function $f: V \rightarrow \mathbb{R}$ provably establishes a quadrangulation of even the most complex surfaces. The *quality* of this quadrangulation, on the other hand, is intimately tied to the choice of function f . Our key insight is that eigenvectors of the Laplacian matrix \mathbf{L} induce scalar fields on the surface that have exactly the right properties necessary to achieve good complexes.

4.1 Laplacian Eigenfields

Any eigenvector \mathbf{e} of \mathbf{L} implicitly determines a function $f: V \rightarrow \mathbb{R}$ over the mesh—the value of f at vertex i is simply the corresponding value e_i in row i of the eigenvector. We refer to this function f , defined by an eigenvector of \mathbf{L} , as an *eigenfield*.

It is well-known that the eigenfields of the Laplacian generalize our usual notion of fixed-frequency functions. The eigenfields of a regular planar grid correspond to the basis functions of the discrete cosine transform, see Figure 3. Similarly, the eigenfields of the sphere produce a discrete form of the spherical harmonics, and they produce discrete toroidal harmonics on the torus. On more general surfaces, the eigenfields continue to define a set of “harmonics” and the corresponding eigenvalues identify their squared frequency.

For our goal of quadrangulation, these eigenfields have several crucial properties. Of greatest importance is the fact that the extrema of the function are distributed in a uniform way; without this property the Morse-Smale complex would produce a very poor quadrangulation. The eigenfields occur in order of increasing frequency,

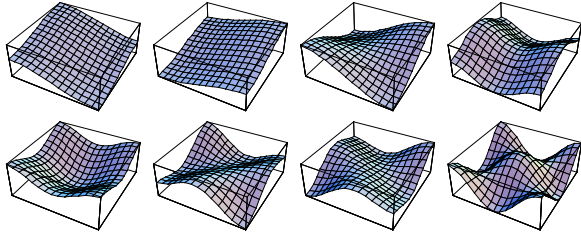


Figure 3: The first 8 non-constant eigenfields over a 15×15 planar grid, plotted as heightfields.

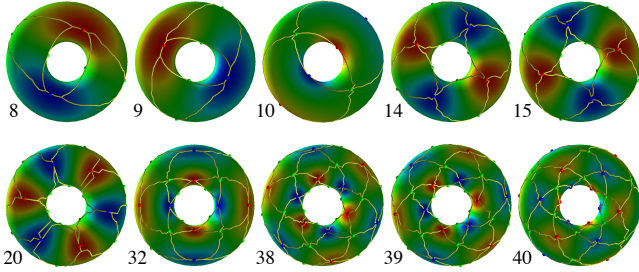


Figure 4: Selected torus eigenfields. Note the increasing complexity and symmetries of higher harmonics.

making it fairly easy to select an eigenfield of a desired complexity. This is also important from an efficiency standpoint, as it means we only need to compute the first k low frequency eigenfields of the matrix. Because it is a fixed-frequency function, the eigenfield is also generally free of superfluous extrema. This keeps the number of extraordinary points low, as only extrema of the eigenfield can be extraordinary points.

We compute eigenfields using the ARPACK sparse eigensystem solver. It implements an iterative Arnoldi method that allows us to efficiently compute only the first k eigenvectors of \mathbf{L} . As we are generally interested in fairly sparse quadrangulations of the surface, we typically need to find only the first 40–60 eigenvectors of \mathbf{L} , regardless of the input mesh complexity.

4.2 Extracting the Morse-Smale Complex

Given a piecewise linear eigenfield defined over the vertices of the mesh, constructing the Morse-Smale complex is straightforward. Starting from each saddle, one computes four steepest lines—two ascending and two descending ones. These *paths* connect the saddle with its surrounding extrema. Two paths in the same direction (both ascending or both descending) can merge; two paths with different directions must remain separate. Once two paths have merged they must never split. After all paths are computed the surface is partitioned into *cells* each of which is incident to two saddles (or the same saddle twice). These conditions are sufficient to guarantee that the complex is in fact a non-degenerate Morse-Smale complex [Bremer et al. 2004]. Note that this algorithm can be defined in a nearly exclusively combinatorial manner, making it simple to implement and stable even for the most degenerate functions.

Figure 4 shows a simple of building Morse-Smale complexes out of successive harmonics (i.e., eigenfields) on a torus. Notice how higher harmonics—corresponding to higher frequencies—produce an increasing number of patches. Also notice the nearly-perfect symmetry of the eigenfields and of the placement of their extrema.

5 Optimizing the Complex

In practice, the initial Morse-Smale complex as computed in Section 4 is not entirely suitable as a quadrangulation of the surface. The numerical eigenvector computation typically generates some amount of noise in the eigenfield, leading to erroneous local extrema. The paths connecting extrema may also be less than satisfactory. They are traced by simple gradient ascent/descent through the field. This has many advantages in terms of correctness and robustness of the topological construction, but it can produce paths that do not follow the surface shape in a natural way. This kind of behavior is clearly evident in the complexes shown in Figure 4.

We address these deficiencies in the complex using a two phase optimization process. First, we optimize the topology of the complex by removing extraneous critical points. Next, we optimize the geometry of the paths in the complex while keeping its connectivity fixed.

5.1 Topology Optimization

Corresponding to spherical harmonics, one expects the eigenfield to be smooth with an increasing number of critical points for increasing eigenvalues. However, the uneven sampling and usually irregular triangulations of the surfaces as well as the iterative eigensolver add noise to the field. Additionally, the combinatorial algorithm used to compute the Morse-Smale complex can add “symbolic” noise due to the arbitrary vertex ordering. Combined, these effects add high frequency distortions which often appear in the Morse-Smale complex as clusters or chains of superfluous critical points, see Figure 5.

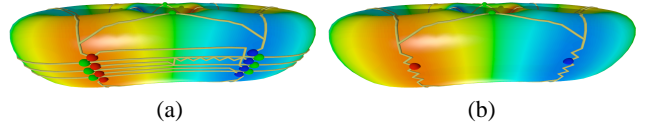


Figure 5: Eigenfield of the three-fold torus. (a) The initial complex showing a typical noise pattern; (b) simplified complex.

To remove the extraneous critical points we use *cancellations* to simplify the Morse-Smale complex [Edelsbrunner et al. 2003; Bremer et al. 2004]. Each cancellation removes a connected saddle-extremum pair, all paths incident to the saddle, and two cells, see Figure 6(a). In general, each saddle can be part of four different cancellations involving either minima or maxima. The only exception are *strangulations*, see Figure 6(b), where a saddle can only be canceled in the direction consisting of two unique extrema. As a graph operation, cancellations can be seen as a slightly more complicated version of an edge collapse. However, following Morse theory, one can also relate cancellations to the corresponding function. First, one defines that for a given saddle and direction (minima/maxima) always the higher minimum or lower maximum must be cancelled. This reduces the number of potential cancellations of a saddle to (at most) two. Second, one ranks cancellations by their *persistence* [Edelsbrunner et al. 2002], defined as the absolute difference in function value of the cancelled pair. A Morse-Smale complex is then simplified by canceling critical points in order of increasing persistence. Conceptually, this algorithm simplifies the Morse-Smale complex indirectly by dealing primarily with the eigenfield itself. In fact, the use of persistence as error metric combined with the greedy simplification approach simulates a topological simplification of the eigenfield. Such an approach has

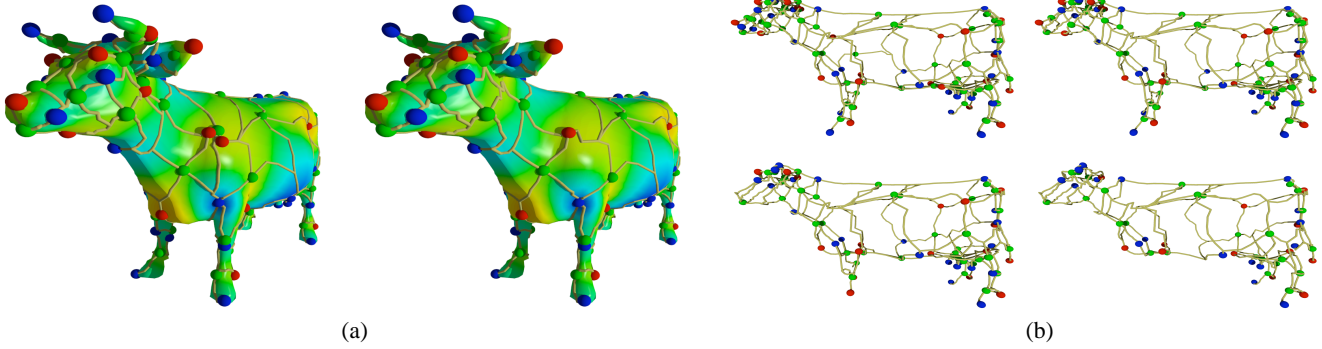


Figure 7: Eigenfield of the cow. (a) Initial complex showing some noise at the shoulder and leg; (b) Complex of (a) simplified with a persistence of 0.3%; (c) The same complex at a persistence of 7% (top-left), 11% (top-right), 15% (bottom-left), and 22% (bottom-right).

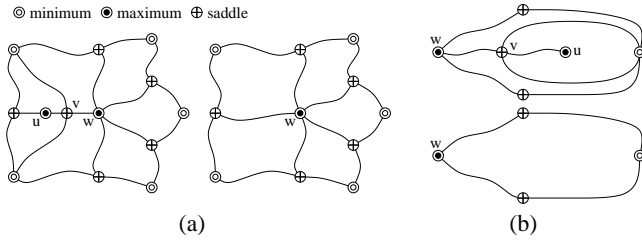


Figure 6: Morse-Smale complex before and after canceling u, v . One saddle and one extremum (maximum) are removed, along with four paths and two (a) or one cells (b). (a) Regular situation allowing v to be cancelled with minima as well as maxima. (b) Strangulation allowing only the cancelation of maxima.

already been proven very effective in removing noise from scientific data [Bremer et al. 2004].

Our experiments show that except for noise the Morse-Smale complexes of certain eigenfields are well suited as base domains. Since the persistence-based simplification removes this noise in a topologically optimal way it is not surprising that simplifying the Morse-Smale complex in this manner performs well. An example is shown in Figure 7 using an eigenfield of the cow mesh. The initial complex already builds an acceptable base complex with critical points at all major geometric features and varying cell size depending on geometric complexity. However, there does exist some noise which would distort an immediate re-meshing. For example, on the right front leg as well as on the side of the left shoulder one can see superfluous critical point pairs (also evident by their asymmetry). With traditional simplification methods these are difficult to remove as for example their geometric distance does not differ much from those on the ears. We have experimented with path-length as well as aspect ratio based simplification schemes but found that these often remove features rather than noise. Figure 7(b) shows the simplified Morse-Smale complex of the cow after canceling all pairs below a persistence of 0.3% (relative to the overall range of the function). Note, that the complex is nearly perfectly symmetrical and transitions naturally between areas of different geometric complexity. Finally, Figure 7(c) shows the same complex more aggressively simplified which produces level-of-detail type complexes. First, the horns are removed (top-left), then the ears (top-right), followed by the front feet (bottom-left), and finally the front legs (bottom-right).

The last step in performing an automatic optimization of an initial complex is to choose an appropriate simplification threshold. As

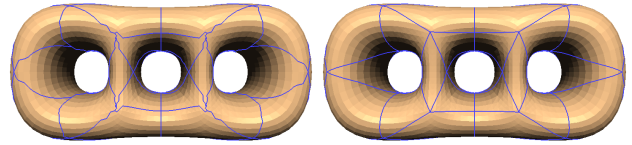


Figure 8: Base complex on the 3-torus before (left) and after (right) path straightening.

the values used in Figure 7 suggest, the amount of noise we have encountered in terms of persistence is minimal. Furthermore, the existing noise is well separated from the “signal” by sometimes several orders of magnitude difference in persistence. Table 1 shows the number of cancellations performed during the clean-up, the noise threshold used, and the smallest persistence of any remaining critical point pair for several data sets. The persistences are measured relative to the maximal function range of the corresponding field.

	bunny	rocker arm	cat	moai	foot
# of cancel.	0	3	5	10	3
thresh. pers.	0%	0.2%	0.6%	0.2%	0.1%
rem. pers.	0.8%	2.3%	6.5%	1.8%	2.8%

Table 1: Number of cancellations performed during clean-up, noise threshold, and smallest remaining persistence.

5.2 Geometry Optimization

The persistence-based simplification that we have just outlined reliably removes what is essentially high-frequency noise in the complex. An additional low-frequency type of noise can be observed once we examine the geometric structure of the complex. In certain rare cases, the complex will contain two nearby saddles that are both connected to far away extrema, as measured by geodesic distance along the surface. This has the effect of producing extremely long and thin diamond shapes. We remove these sliver patches by merging the two saddles in question into a single higher order saddle. As with the persistence-based simplification, there is a wide and easily detected separation between these undesirable saddles and normal saddles.

Once the connectivity of the complex is fixed, we proceed to optimize the geometry of its paths. During the initial complex construc-

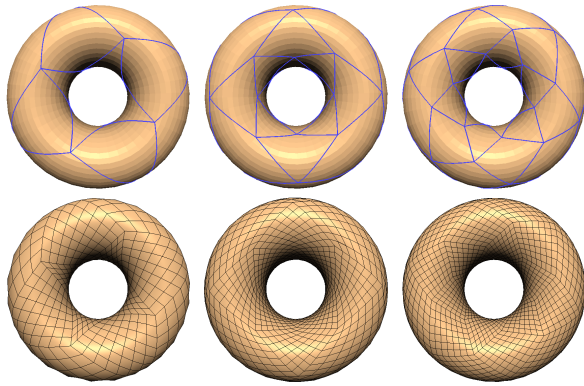


Figure 9: Remeshing the torus with progressively higher harmonics. Note the near-perfect symmetry of the quadrangulations.

tion, the paths are extracted by following gradient ascent/descent lines through the eigenfield. This can produce rather jagged paths, especially when the input mesh is poorly tessellated. We would like to replace each path with a “straightened” version.

We formulate the problem as one of tracing a straightest geodesic path [Polthier and Schmies 1998] between adjacent nodes in the complex, subject to the constraint that paths may never cross. Because of this constraint, we do not actually use a global algorithm such as that proposed by Polthier and Schmies because guaranteeing the validity of the paths can become extremely difficult. Instead, we opt to iteratively straighten a local section of a given path contained within the 1-ring of a selected vertex. This restricted local update allows us to easily guarantee that the paths of the complex will never cross, which would result in an invalid complex. It is not necessarily guaranteed to converge to the optimal geodesic curve, but this is of far less importance than preserving the correctness of the complex. An example of the straightening process is shown in Figure 8.

6 Results

In this section, we investigate the results achieved in practice by our quadrangulation technique. We illustrate the behavior of our quadrangulations by using them as base complexes for semi-regular remeshing of the input surface.

We intentionally adopt a very simple approach to producing a semi-regular mesh from our quadrangular base complexes. The user specifies a desired sampling rate d . We then parameterize each patch onto the unit square $[0, 1] \times [0, 1]$ using a simple linear method that is guaranteed to be valid [Floater 2003]. Once a patch is parameterized, we construct a regular $d \times d$ grid of quadrilaterals in this parametric domain, and map their corners back onto the surface to produce our output mesh. By sampling at a fixed rate we trivially guarantee that the final mesh is fully conforming. The quality of meshes produced by this simple resampling scheme is completely dependent on the quality of the base complex produced by our algorithm. As we shall see, we are indeed able to produce good quality meshes in this manner, thus demonstrating the quality of our underlying quadrangulation. By using this regular sampling scheme, we also guarantee that extraordinary points can only occur at extrema of the eigenfield.

For our first example, shown in Figure 9, we look at our results on a torus. This is a simple surface whose eigenfields, as we have men-

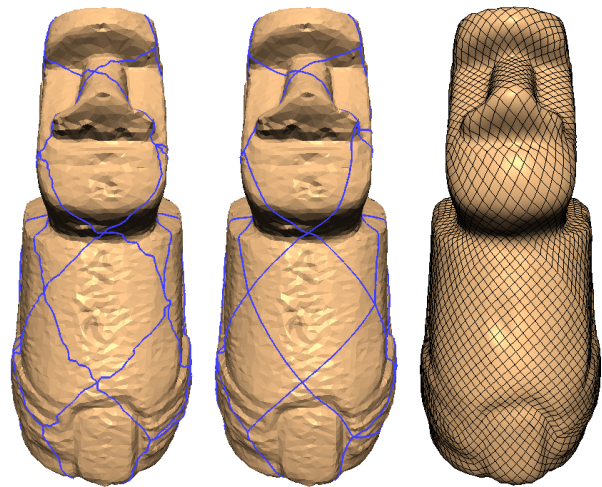


Figure 10: We optimize the raw Morse-Smale complex (left), producing a straightened complex (middle) from which we extract a semi-regular quad mesh (right).

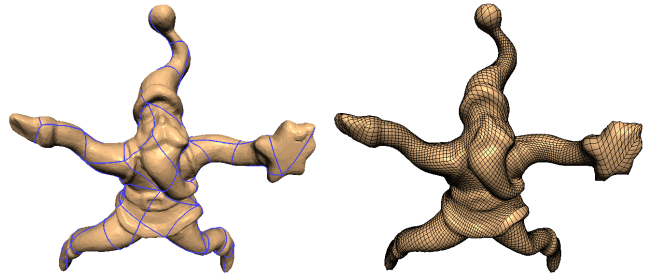


Figure 11: The base complex, and hence the remesh, captures the protrusions of this mesh quite well.

tioned earlier, are discretizations of continuous toroidal harmonics. The spectrum of the torus is in fact highly structured, and the eigenfields and complexes we extract exhibit near-perfect symmetry. This regularity and symmetry are apparent in the remeshing output as well. Note that while the torus can be tessellated with a fully regular quad mesh, our method does not produce such meshes. Rather, the number of extraordinary points is related to the harmonic chosen to determine the base complex.

Figure 10 shows a quadrangulation of a scanned Moai statue. The raw surface data (on which the complex is superimposed) is fairly noisy and the mesh is moderately irregular. Nevertheless, the quadrangulation is quite stable and the straightened complex provides a good decomposition of the surface. The remeshing result is quite uniform and the individual elements are generally very well-shaped.

Further remeshing results can be seen on the bunny in Figure 1, the Santa ornament in Figure 11, and the rocker arm in Figure 12. These surfaces all exhibit fairly complex geometry, which our quadrangulation is able to capture and preserve during resampling. Both the bunny and the Santa ornament have significant features protruding from the main body of the surface. If these are not captured well by the base complex, our regular remeshing procedure would produce very high parametric distortions — and hence very poor meshes — in these areas. However, we see that the surface is covered at a fairly uniform rate, indicating that the base complex

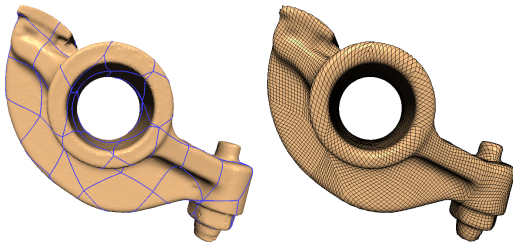


Figure 12: Remeshing a more complex genus-1 surface.

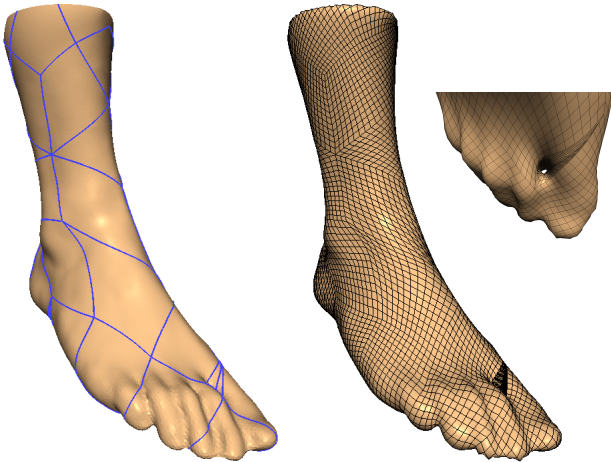


Figure 13: This foot is a smooth surface, and is sampled with a fairly uniform mesh. Our method also correctly handles the tiny topological hole in the toes.

has done a good job of identifying and capturing these features. Similarly, the rocker arm contains a large topological handle which can, with a poor base complex, degenerate terribly when remeshed. Again, we see that our base complex and the derived remeshing result samples this feature quite well.

Next let us consider the foot shown in Figure 13. This surface clearly ought to be of genus 0. However, as the result of reconstruction errors, it is actually genus 1. There is a very small topological handle between the first two toes. This kind of topological “noise” can be difficult to detect, and many methods do not handle it well. In contrast, our quadrangulation approach is based on a theoretically robust procedure for extracting the topology of the surface. It correctly handles this tiny topological feature by threading the quadrangulation through the hole.

A currently popular scheme for remeshing surfaces with quadrilaterals is based on tracing two families of mutually orthogonal integral lines over the surface [Alliez et al. 2003a; Marinov and Kobbelt 2004; Dong et al. 2005]. The intersections of these lines are used to determine vertex placement, and the spacing between lines is controlled by locally starting/stopping flow lines. We illustrate the results of one such system, implementing a method like the one described by Dong et al. [2005], in Figure 14. On the left is a mesh that tries to maintain a uniform edge length everywhere, and on the right is a mesh that attempts to vary interline spacing based on the local surface curvature. Compare these two meshes with the result shown in Figure 1 produced by our system. All 3 meshes contain roughly 9800 vertices. First, tracing schemes produce quad-dominant rather than pure quad meshes. Because they control mesh density by starting and terminating flow lines over

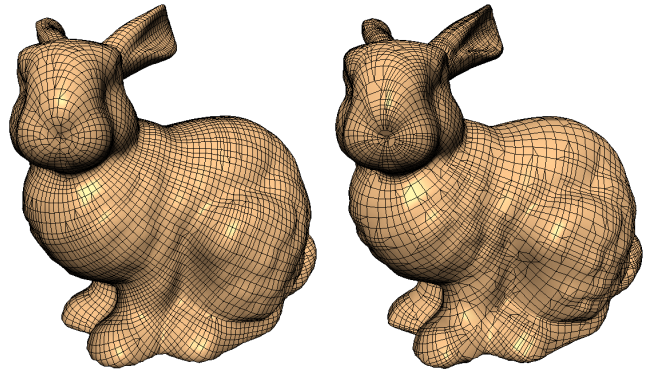


Figure 14: Quad meshes produced by line tracing algorithms produce much more irregular meshes, especially when trying to locally adapt to surface curvature (at right).

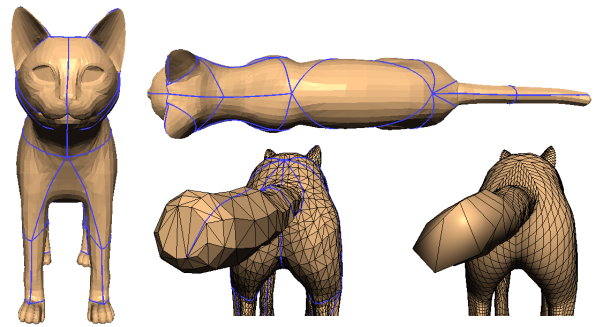


Figure 15: The eigenfield complex detects both symmetries and protrusions. However, the tail is distorted because the input mesh has no vertex at the tip.

the surface, they also produce noticeably more irregularities in the mesh. This effect is particularly pronounced when trying to adapt the spacing to local surface curvature. As the curvature estimates vary over the surface, flow lines are frequently stopped and started. Each such decision produces an irregularity in the mesh. The cumulative effect is a significantly irregular mesh. Similar effects can be seen in the results reported by Alliez et al. [2003a], Marinov and Kobbelt [2004], and Dong et al. [2005]. In contrast, our meshes generally have few extraordinary points.

Now let us consider the cat shown in Figure 15. It is clear that the base complex does an excellent job of capturing the symmetry of the surface. It also does a very good job of capturing the protruding limbs and ears — except the tail. As we can see, the remeshing of the tail is rather distorted. This illustrates one limitation of our approach. The Laplacian eigenfields reliably contain extrema at the tips of protruding features. However, by construction extrema may only occur at vertices of the input mesh. The original cat mesh has no vertex at the tip of the tail, and thus our method is not able to place a base complex vertex at the ideal location on the tip of the tail. Instead, we can see it is forced to use a nearby vertex.

The remeshing results we have shown up to this point are rendered as simple bilinear quadrilaterals. To get a clearer picture of the geometric fidelity of these meshes, we show several of these meshes rendered as Catmull-Clark surfaces in Figure 16. These surfaces clearly capture the geometry of the original datasets quite well. The only noticeable artifacts are a few very small ripples in the surfaces, which are mainly due to the fact that we do not enforce parametric

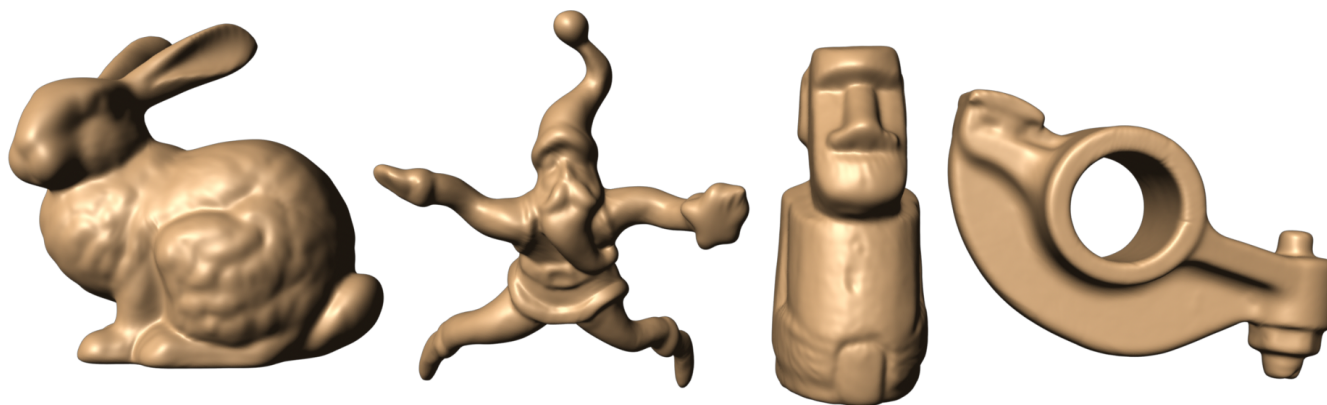


Figure 16: Selected remeshing results from previous figures rendered as Catmull-Clark surfaces.

continuity between patches.

For all the examples that we have shown, eigenvector extraction is by far the dominant cost. The time necessary to extract the first 60 eigenvectors, which is the maximum extent of the spectrum used in any example, ranged from 2 to 25 minutes. Computing and simplifying the initial Morse-Smale complex took less than 2 seconds, optimizing a single complex at most 20 seconds, and the time to parameterize and resample the mesh was 5 seconds or less. Note that the efficiency of the eigenvector extraction could be improved dramatically by using a hierarchical eigenvector solver [Barnard and Simon 1994; Koren et al. 2002].

7 Discussion

Spectral Partitioning. A number of spectral graph partitioning methods have been proposed in the past. The focus of the majority of this work has been on spectral bisection of graphs. The Fiedler vector assigns a scalar value to each vertex, and we can bisect the graph by partitioning the vertices based on whether they are above or below the median field value. A handful of methods have been developed to accelerate this process by using the first k Laplacian eigenvectors [Hendrickson and Leland 1995; Liu and Zhang 2004]. While ours is also a spectral partitioning algorithm, it is fundamentally quite different. The results produced by spectral bisection, and its generalizations, are much more closely related to the graphcut decompositions of Katz *et al.* [2003].

Morse Analysis of Eigenfields. While Morse theory is certainly not novel using it to analyze eigenfields has proven to be surprisingly effective. The critical points are typically distributed according to geometric complexity without neglecting areas of low or constant curvature. This results in Morse-Smale complexes which transition smoothly between region of different geometric detail but always provide a sufficiently dense base complex. Additionally, the persistence based simplification performs nearly optimal in both detecting noise as well as in choosing which vertices to remove. Finally, considering the rather involved mathematical procedures used to compute eigenfields it is interesting to note that the eigenfields contain a remarkably low amount of high frequency noise.

Remeshing Limitations. It is important to understand the practical limitations of the proof-of-concept remeshing method that we have presented. Like most methods arising from the computer

graphics literature, we do not provide any firm guarantees on element quality (e.g., minimum angle). Therefore, this method may not be suitable for use in finite element methods where such guarantees are critical for success. While our choice of a simple linear parameterization scheme suits our expository goal of not artificially correcting for problems in the base complex, it results in more parametric distortion than is absolutely necessary. For real-world use, we recommend more sophisticated non-linear methods. Similarly, we have used a “blind” semi-regular remeshing scheme that lays down a uniform grid of quadrilaterals in the parametric domain without regard for the shape of the surface. Optimizing the placement of individual vertices could significantly improve the quality of the output surfaces. There may also be cases where allowing extraordinary points to occur on the interior of patches would, in practice, improve the fidelity to the original shape.

8 Conclusions

In this paper, we have outlined a new theoretical framework for quadrangulating polygonal manifolds. By using Morse theory to analyze the structure of the Laplacian eigenfields of the surface, we are able to produce appealing quadrangulations that arise directly from the intrinsic shape of the manifold. Our use of the Morse-Smale complex is topologically robust and guarantees that the base complex is always quadrangular. We have also demonstrated that the resulting base complexes are well-suited for remeshing the input with a fully conforming semi-regular mesh consisting entirely of quadrilaterals.

The results we have presented in this paper open a new line of research aimed at describing and understanding shapes and geometry. We have chosen semi-regular quadrangular remeshing as an example which demonstrates that the Morse-Smale structure of Laplacian eigenfields encodes fundamental information about the shape of a piecewise linear manifold. But more broadly, these results are based on several intriguing properties of the Laplace matrix and its eigenfields that we have only begun to explore.

There is much that could be learned from a more thorough theoretical understanding of the structure of the Laplacian spectrum. The majority of results in spectral graph theory tie the Laplacian eigenvalues to various properties of the graph. The structure of the eigenvectors is relatively unexplored. A clearer understanding of the spectral structure should enable us to prove stronger results about the quality of the final quadrangulation.

We have noted that persistence-based simplification of the eigenfields, as shown in Fig. 7, produces an appealing multiresolution structure over the surface. Exploring the nature of this structure, and its relation to the nesting of eigenfields of different frequencies should prove valuable.

The optimization of the base complex geometry is also an area that seems ripe for potentially fruitful improvement. Our current optimization procedure is focused on straightening and smoothing the paths which form the complex. Ultimately, the primary goal of this optimization is to minimize parametric distortion within the patch. A scheme to directly minimize this distortion should produce even better base complexes. It would also be worthwhile to explore techniques for ensuring global parametric continuity. Finally, we believe it would be beneficial to consider locally optimizing the placement of critical points as their position, like the paths connecting them, may be perturbed by the presence of noise in the eigenfield.

References

- ALLIEZ, P., MEYER, M., AND DESBRUN, M. 2002. Interactive geometry remeshing. *TOG 21*, 3, 347–354. (Proc. SIGGRAPH).
- ALLIEZ, P., COHEN-STEINER, D., DEVILLERS, O., LÉVY, B., AND DESBRUN, M. 2003. Anisotropic polygonal remeshing. *TOG 22*, 3, 485–493.
- ALLIEZ, P., DE VERDIÈRE, É. C., DEVILLERS, O., AND ISENBURG, M. 2003. Isotropic surface remeshing. In *Proc. Shape Modeling Intl.*, 49–58.
- ATKINS, J. E., BOMAN, E. G., AND HENDRICKSON, B. 1999. A spectral algorithm for seriation and the consecutive ones problem. *SIAM J. on Comp.* 28, 1, 297–310.
- BANCHOFF, T. F. 1967. Critical points and curvature for embedded polyhedral surfaces. *Differential Geometry 3*, 1, 257–268.
- BARNARD, S. T., AND SIMON, H. D. 1994. A fast multilevel implementation of recursive spectral bisection for partitioning unstructured problems. *Concurrency Practice & Experience 6*, 101–117.
- BERN, M. W., AND EPPSTEIN, D. 1995. Mesh generation and optimal triangulation. In *Computing in Euclidean Geometry*, D.-Z. Du and F. K. Hwang, Eds., Lecture Notes on Computing #4. World Scientific, 47–123.
- BOIER-MARTIN, I., RUSHMEIER, H., AND JIN, J. 2004. Parameterization of triangle meshes over quadrilateral domains. In *Proc. Eurographics Symposium on Geometry Processing*, 197–207.
- BREMER, P. T., EDELSBRUNNER, H., HAMANN, B., AND PASCUCCI, V. 2004. A topological hierarchy for functions on triangulated surfaces. *TVCG 10*, 4, 385–396.
- CAYLEY, A. 1859. On contour and slope lines. *The London, Edinburgh & Dublin Phil. Mag. & J. of Sci.* XVIII, 264–268.
- CHUNG, F. R. K. 1997. *Spectral Graph Theory*. American Mathematical Society.
- COHEN-STEINER, D., ALLIEZ, P., AND DESBRUN, M. 2004. Variational shape approximation. *TOG 23*, 3, 905–914. (Proc. SIGGRAPH).
- DESBRUN, M., MEYER, M., SCHRÖDER, P., AND BARR, A. H. 1999. Implicit fairing of irregular meshes using diffusion and curvature flow. In *Proc. SIGGRAPH*, 317–324.
- DONG, S., KIRCHER, S., AND GARLAND, M. 2005. Harmonic functions for quadrilateral remeshing of arbitrary manifolds. *CAGD*. To appear.
- DUCHAMP, T., CERTAIN, A., DEROSE, A., AND STUETZLE, W. 1997. Hierarchical computation of PL harmonic embeddings. preprint.
- ECK, M., AND HOPPE, H. 1996. Automatic reconstruction of B-spline surfaces of arbitrary topological type. In *Proc. SIGGRAPH*, 325–334.
- ECK, M., DEROSE, T. D., DUCHAMP, T., HOPPE, H., LOUNSBERY, M., AND STUETZLE, W. 1995. Multiresolution analysis of arbitrary meshes. In *Proc. SIGGRAPH*, 173–182.
- EDELSBRUNNER, H., AND MÜCKE, E. P. 1990. Simulation of simplicity: A technique to cope with degenerate cases in geometric algorithms. *TOG 9*, 66–104.
- EDELSBRUNNER, H., LETSCHER, D., AND ZOMORODIAN, A. 2002. Topological persistence and simplification. *Discrete Comput. Geom.* 28, 511–533.
- EDELSBRUNNER, H., HARER, J., AND ZOMORODIAN, A. 2003. Hierarchical Morse-Smale complexes for piecewise linear 2-manifolds. *Discrete Comput. Geom.* 30, 87–107.
- FLOATER, M. S., AND HORMANN, K. 2004. Surface parameterization: a tutorial and survey. In *Multiresolution in Geometric Modelling*, N. A. Dodgson, M. S. Floater, and M. A. Sabin, Eds. Springer.
- FLOATER, M. S. 2003. Mean value coordinates. *Computer Aided Geometric Design* 20, 1 (Mar.), 19–27.
- FRIEDEL, I., SCHRÖDER, P., AND KHODAKOVSKY, A. 2004. Variational normal meshes. *TOG 23*, 4, 1061–1073. (Proc. SIGGRAPH).
- GARLAND, M., AND HECKBERT, P. S. 1997. Surface simplification using quadric error metrics. In *Proc. SIGGRAPH*, 209–216.
- GARLAND, M., WILLMOTT, A., AND HECKBERT, P. S. 2001. Hierarchical face clustering on polygonal surfaces. In *Proc. Symp. Interactive 3D Graphics*, 49–58, 245.
- GARLAND, M. 1999. Multiresolution modeling: Survey & future opportunities. In *State of the Art Report*, Eurographics, 111–131.
- GU, X., GORTLER, S. J., AND HOPPE, H. 2002. Geometry images. *TOG 21*, 3, 355–361. (Proc. SIGGRAPH).
- GUSKOV, I., VIDMCE, K., SWELDENS, W., AND SCHRÖDER, P. 2000. Normal meshes. In *Proc. SIGGRAPH*, 95–102.
- HENDRICKSON, B., AND LELAND, R. 1995. An improved spectral graph partitioning algorithm for mapping parallel computations. *SIAM J. Sci. Comp.* 16, 2, 452–469.
- HILAGA, M., SHINAGAWA, Y., KOHURA, T., AND KUNII, T. L. 2001. Topology matching for fully automatic similarity estimation of 3d shapes. In *Proc. SIGGRAPH*, 203–212.
- HOPPE, H., DEROSE, T., DUCHAMP, T., McDONALD, J., AND STUETZLE, W. 1993. Mesh optimization. In *Proc. SIGGRAPH*, 19–26.
- HOPPE, H. 1996. Progressive meshes. In *Proc. SIGGRAPH*, 99–108.
- ISENBURG, M., AND LINDSTROM, P. 2004. Streaming meshes. Tech. Rep. UCRL-CONF-201992, Lawrence Livermore Natl. Lab.
- KALVIN, A. D., AND TAYLOR, R. H. 1996. Surfaces: Polygonal mesh simplification with bounded error. *CG&A 16*, 3, 64–77.
- KARNI, Z., AND GOTSMAN, C. 2000. Spectral compression of mesh geometry. In *Proc. SIGGRAPH*, 279–286.
- KATZ, S., AND TAL, A. 2003. Hierarchical mesh decomposition using fuzzy clustering and cuts. *TOG 22*, 3, 954–961. (Proc. SIGGRAPH).
- KHODAKOVSKY, A., LITKE, N., AND SCHRÖDER, P. 2003. Globally smooth parameterizations with low distortion. *TOG 22*, 3, 350–357. Proc. SIGGRAPH.
- KOREN, Y., CARMEL, L., AND HAREL, D. 2002. ACE: A fast multiscale eigenvectors computation for drawing huge graphs. In *Proc. InfoVis '02*, 137–144.
- LEE, A. W. F., SWELDENS, W., SCHRÖDER, P., COWSAR, L., AND DOBKIN, D. 1998. MAPS: Multiresolution adaptive parameterization of surfaces. In *Proc. SIGGRAPH*, 95–104.
- LIU, R., AND ZHANG, H. 2004. Segmentation of 3D meshes through spectral clustering. In *Proc. Pacific Graphics '04*, 298–305.
- MARINOV, M., AND KOBBELT, L. 2004. Direct anisotropic quad-dominant remeshing. In *Proc. Pac. Graphics*.
- MAXWELL, J. C. 1870. On hills and dales. *The London, Edinburgh & Dublin Phil. Mag. & J. of Sci.* XL, 421–427.
- MILNOR, J. 1963. *Morse Theory*. Princeton University Press.
- MORSE, M. 1925. Relations between the critical points of a real functions of n independent variables. *Trans. AMS* 27, 345–396.
- NI, X., GARLAND, M., AND HART, J. C. 2004. Fair Morse functions for extracting the topological structure of a surface mesh. *TOG 23*, 3, 613–622. (Proc. SIGGRAPH).
- OWEN, S., STATEN, M. L., CANANN, S. A., AND SAIGAL, S. 1999. Q-Morph: An indirect approach to advancing front quad meshing. *Intl. Journal for Numerical Methods in Engineering* 9, 1317–1340.
- OWEN, S. J. 1998. A survey of unstructured mesh generation technology. In *Proc. Meshing Roundtable*.
- PASCUCCI, V., AND COLE-MCLAUGHLIN, K. 2002. Efficient computation of the topology of level sets. In *Proc. Visualization*, 187–194.
- PINKALL, U., AND POLTHIER, K. 1993. Computing discrete minimal surfaces and their conjugates. *Exp. Math.* 2, 1, 15–36.
- POLTHIER, K., AND SCHMIES, M. 1998. Straightest geodesics on polyhedral surfaces. *Mathematical Visualization*, 135–150.
- SANDER, P. V., WOOD, Z. J., GORTLER, S. J., SNYDER, J., AND HOPPE, H. 2003. Multi-chart geometry images. In *Proc. Eurographics Symposium on Geometry Processing*, Eurographics Association, 146–155.
- SCHROEDER, W. J., ZARGE, J. A., AND LORENSEN, W. E. 1992. Decimation of triangle meshes. *Computer Graphics* 26, 2 (July), 65–70. (Proc. SIGGRAPH).
- SHIMADA, K., LIAO, J.-H., AND ITOH, T. 1998. Quadrilateral meshing with directionality control through the packing of square cells. In *Seventh Intl. Meshing Roundtable*, 61–75.
- STANDER, B. T., AND HART, J. C. 1997. Guaranteeing the topology of implicit surface polygonization for interactive modeling. In *Proc. SIGGRAPH*, 279–286.
- SURAZHISKY, V., AND GOTSMAN, C. 2003. Explicit surface remeshing. In *Proc. Symp. on Geometry Processing*, 20–30.
- SURAZHISKY, V., ALLIEZ, P., AND GOTSMAN, C. 2003. Isotropic remeshing of surfaces: A local parameterization approach. In *Proc. Meshing Roundtable*.
- TAUBIN, G. 2000. Geometric signal processing on polygonal meshes. In *State of the Art Report*, Eurographics, 81–96.
- TURK, G. 1992. Re-tiling polygonal surfaces. *Computer Graphics* 26, 2, 55–64. (Proc. SIGGRAPH).
- VAN KREVELD, M. J., VAN OOSTRUM, R., BAJAJ, C. L., PASCUCCI, V., AND SCHIKORE, D. 1997. Contour trees and small seed sets for isosurface traversal. In *Symp. Comp. Geom.*, 212–220.
- WEBER, G., SCHEUERMANN, G., HAGEN, H., AND HAMANN, B. 2002. Exploring scalar fields using critical isovalues. In *Proc. Visualization*, 171–178.
- WHITE, D. R., AND KINNEY, P. 1997. Redesign of the paving algorithm: Robustness enhancements through element by element meshing. In *Proc. Meshing Roundtable*, 323–335.